RSC Advances

ROYAL SOCIETY OF CHEMISTRY

www.rsc.org/advances

The effect of microstructure and surface decoration with K_2NiF_4-type oxide upon the oxygen permeability of perovskite-type $La_{0.7}Sr_{0.3}FeO_{3-\delta}$ hollow fiber membranes

Ning Han,[†] Shuguang Zhang,[*,†] Bo Meng,[†] Xiaoyao Tan,[*,‡]

[†] *School of Chemical Engineering, Shandong University of Technology, Zibo 255049, China*

[‡] *Department of Chemical Engineering, Tianjin Polytechnic University, Tianjin 300387, China*

[*] *Corresponding author. E-mail: gregzhangsg@gmail.com(S. Zhang), cestanxy@aliyun.com(X. Tan).*

Abstract: Dense $La_{0.7}Sr_{0.3}FeO_{3-\delta}$ (LSF) hollow fiber membranes with two kinds of microstructures (LSF-a and LSF-b) were prepared by the phase inversion/sintering method. Outer surface decoration with dispersed porous K_2NiF_4-type oxide $(La_{0.5}Sr_{0.5})_2CoO_{4+\delta}$ (LSC_{214}) was employed to improve the surface exchange reaction kinetics of oxygen reduction. Experimental results suggest the oxygen permeability of the LSF-b membrane is much better than that of LSF-a membrane at all the tested conditions, which means the microstructure of the hollow fiber membrane plays a crucial role in the oxygen permeability. LSC_{214} decoration further increases the oxygen permeation flux greatly. Moreover, although the oxygen permeation fluxes are positively related to both the operating temperature and flow rate of helium gas, the former has a greater effect on the oxygen permeation performance than the latter. Keeping the flow rate of helium gas at 200 $ml \cdot min^{-1}$, the oxygen permeation fluxes of the bare LSF-a (LSF-b) and the LSC_{214}-decorated LSF-a (LSF-b) membranes are about 0.009-0.367 (0.254-5.401) and 0.048-0.426 (1.520-7.003) $ml \cdot min^{-1} \cdot cm^{-2}$, respectively, with operating temperature varied from 700 to 1000 °C. For both kinds of decorated membranes, more remarkable improvements of oxygen permeation fluxes appear at intermediate operating temperature range (700-850 °C) than higher temperature range (850-1000 °C), which indicates that the surface oxygen exchange reaction plays a decisive role in controlling the overall oxygen transport process at lower temperature. In addition, the surface decorated membrane also displays high permeation stability under the investigated operating conditions.

Key words: hollow fiber membrane, microstructure, oxygen permeability, K_2NiF_4-type oxide,

dispersed surface decoration

1. Introduction

Oxygen is one of the most important chemicals at present as its applications relate to almost every sector in our economy from chemical industry, metal manufacturing, medical/health care, space/military industry, and the huge newly emerging markets of clean energy industry for carbon capture and storage.[1,2] Unfortunately, current large-scale industrial oxygen production is still carried out by cryogenic distillation process, an expensive technology. Thus, it is quite urgent to find a new cost-effective and environment-friendly technology to replace the conventional one.

Ceramic membrane of mixed oxygen ionic and electronic conductors (MIEC) have gained significant interests due to its high selectivity, high energy conversion efficiency, cost-efficient, eco-friendly in O_2 production process.[3-12,] Although small pilot scale facilities associated with this ceramic membrane technology have been set up by Air Product and Chemicals Inc., extensive applications have been restricted greatly by the poor oxygen permeability, material stability and the high operating temperature. Among the MIEC membranes studied, ABO_3-type perovskite oxides are the focus of research.[13-15] Specifically, $La_{0.6}Sr_{0.4}Co_{0.2}Fe_{0.8}O_{3-\delta}$, one of the most typical perovskite materials, has been widely investigated as oxygen separation membrane and solid oxide fuel cells (SOFC) cathode material because of its intermediate oxygen permeability and relatively high stability. However, it is well known that cobalt is easy to run away from the perovsikte bulk material during the oxygen separation process, resulting in the degradation of this material. Consequently, in this work, $La_{0.7}Sr_{0.3}FeO_{3-\delta}$ has been selected as the membrane substrate to demonstrate the improvement of the oxygen permeability by surface decoration strategy.

For a dense membrane made from a certain material, the oxygen concentration gradient across the membrane and the entire resistance of bulk diffusion and surface exchange processes are the two major factors which may affect the oxygen permeability.[16-18] Keeping a constant oxygen concentration gradient, surface exchange reaction controls the oxygen permeation process at lower

temperature, while bulk diffusion process gradually predominates it with the increase of temperature. Hence the oxygen permeability could be improved greatly by reducing membrane thickness or surface modification.[19-21] Owing to the structure characteristics of perovskite hollow fiber membranes prepared in this work, the oxygen permeability may be more significantly limited by the surface exchange reaction occurring at the gas/solid interface. Then the oxygen permeation can be effectively improved by enhancing the oxygen surface exchange kinetics, which could be realized traditionally by coating a second phase with superior oxygen exchange activity to the membrane surface to trigger a faster oxygen exchange reaction (Fig.1(b)).[20,22] To further extend the triple-phase boundary (TPB) greatly, dispersed-second-phase particle decoration, a new surface modification method, was adopted here, as shown in Fig.1(c). Undecorated systems were also investigated for comparison purpose.

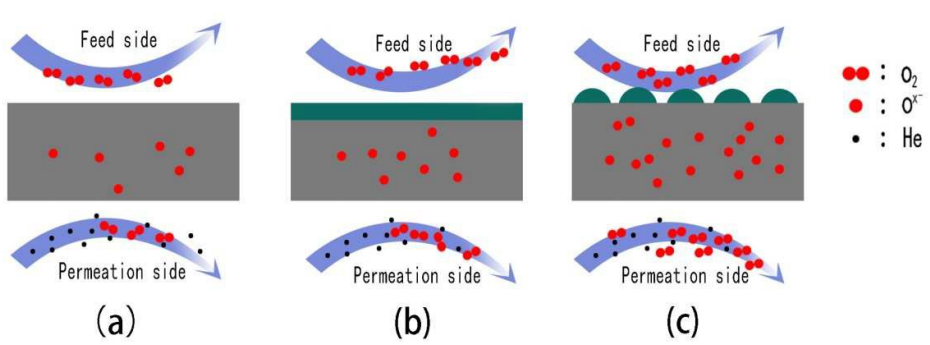

Fig.1. Schematic of membrane surface treatment: (a) bare/untreated membrane; (b) surface modified with a second-phase intact layer; (c) surface decorated with dispersed-second-phase particles.

Besides the two factors mentioned above, microstructure of the hollow fiber membrane also influences the oxygen permeability greatly, sometimes it even plays a decisive role. $La_{0.7}Sr_{0.3}FeO_{3-\delta}$ hollow fiber membranes with two typical microstructures were prepared in this study: symmetrical sandwich structure in Fig.2(a) and asymmetrical structure with long finger-like pores in Fig.2(b), the former consists of three dense layers and two finger-like pores layers, whereas the latter owns only one long finger-like pores layer extending to the inner surface straightly and one dense layer on the outer surface of the membrane, facilitating oxygen permeation process by reducing the surface oxygen exchange reaction times and improving the bulk diffusion of oxygen ions.

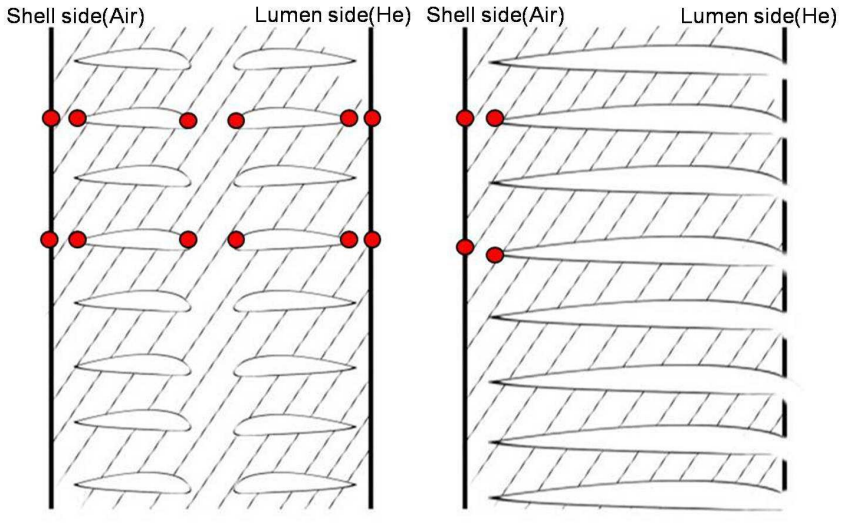

(a) sandwich structure (b) asymmetrical structure

Fig.2. Schematic diagram of two typical wall microstructures of $La_{0.7}Sr_{0.3}FeO_{3-\delta}$ membranes. (surface reaction sites marked with red circles)

In this work, $La_{0.7}Sr_{0.3}FeO_{3-\delta}$ (LSF) hollow fiber membrane was chosen as the substrate and $(La_{0.5}Sr_{0.5})_2CoO_{4+\delta}$, a K_2NiF_4-type oxide, was used as the surface decoration catalyst to improve the surface oxygen reduction reaction (ORR) of LSF membrane for oxygen separation.[23-28] Gas-tight LSF hollow fiber membranes with different microstructures were prepared through the phase inversion/sintering technique to probe the resistance of oxygen permeation process.[29] Then a discontinuous porous thin layer of $(La_{0.5}Sr_{0.5})_2CoO_{4+\delta}$ was deposited on the outer surface of the membranes. The influence of surface decoration on the oxygen permeability of both kinds of LSF hollow fiber membranes was investigated experimentally and the corresponding mechanism was also discussed in detail.

2. Experimental section

2.1 Preparation of powders

The powders of perovskite $La_{0.7}Sr_{0.3}FeO_{3-\delta}$ (hereinafter referred to as LSF) and perovskite-like $(La_{0.5}Sr_{0.5})_2CoO_{4+\delta}$ (hereinafter referred to as LSC_{214}) were synthesized through a combined citric acid-ethylene glycol complexing method, i.e. the so-called Pechini sol–gel method.[30,31] Taking the synthesis of LSF as an example, stoichiometric amount of $La(NO_3)_3 \cdot 6H_2O$, $Sr(NO_3)_2$ and $Fe(NO_3)_3 \cdot 9H_2O$ were dissolved in deionized water to form an aqueous solution, and then citric acid

and ethylene glycol were added with the mole ratio of 1.5:1.8:1 ($n_{\text{citric acid}}$: $n_{\text{ethylene glycol}}$: $n_{\text{metal ions}}$). The mixture was then evaporated at 70 °C under continuous stirring to remove excessive water until a viscous gel was obtained. The gel was then transferred to a container placed on a hot plate. Further heating was conducted till self-combustion occurred to form precursor of LSF powder. The as-synthesized LSF powder was subsequently calcined at 800 °C for 4 h to remove the residual carbon and obtain the desired LSF material with perovskite structure. In order to facilitate the subsequent hollow fiber membrane preparation, the calcined LSF powder was ground and crushed in ethanol with a planet-type ball mill for 24 h, followed by sieving through a sifter of 200-mesh to exclude agglomerates. The K_2NiF_4-type oxide LSC_{214} powder was prepared in a similar way.

2.2 Fabrication of LSF hollow fiber membranes

The LSF hollow fiber membrane precursors were fabricated with the calcined and ball-milled LSF powder by the phase inversion-sintering method.[29] In this work, the spinning mixture was composed of 66.7 wt% calcined LSF powder, 6.60 wt% polyethersulfone (PESf) and 26.7 wt% 1-methyl-2-pyrrolidinone (NMP). At room temperature, the viscosity of the spinning mixture was measured as 11800 mPa·s at the shear rate of 3 rpm. A spinneret with the orifice diameter/inner diameter of 3.0/1.2 mm was used. Deionized water and 30wt%EtOH/70wt%NMP were used as the internal coagulants alternatively, and tap water was adopted as external coagulants. Two kinds of membrane structures were produced finally: (a) symmetrical sandwich structure in Fig.1(a) (internal coagulant: deionized water), hereinafter referred to as LSF-a; (b) asymmetrical structure with long finger-like pores in Fig.1(b) (internal coagulant: 30wt%EtOH/70wt%NMP), hereinafter referred to as LSF-b. After drying, the hollow fiber precursors were sintered at 1350 °C for 4 h to obtain the dense hollow fiber membranes. The gas-tightness of the hollow fibers was evaluated by nitrogen leakage experiment.[32]

2.3 Outer surface decoration of LSF hollow fiber membranes

A controlled dip-coating method was employed to deposit the perovskite-like LSC_{214} oxide powder onto the outer surface of LSF hollow fiber membranes. The thickness of LSC_{214} decoration layer could be modulated by changing the particle loading of coating slurry (Table 1) as well as immersion times.

Table 1. Formula of the LSC_{214} slurry for surface modification

Experimental parameters	Values
Compositions of the slurry	
$(La_{0.5}Sr_{0.5})_2CoO_{4+\delta}$ powder	15 wt%
2 - butanone	26.7 wt%
ethanol	53.3 wt%
triethanolamine (TEA, Mw:149)	0.5 wt%
polyvinyl butyral(PVB, Mw:300)	2 wt%
polyethylene glycol(PEG, Mw:380-420)	0.5 wt%
dibutyl phthalate(DBP, Mw:278)	0.5 wt%
high purity graphite(Size: 80 mesh)	1.5%
Ball-milling time	48 h
Dipping times	One
Pulling speed	60 $mm \cdot min^{-1}$

2.4 Oxygen permeation measurement

The apparatus of oxygen permeation test consists of gas supply, gas flow control, permeation reactor module with furnace and gas chromatography. Oxygen permeation performance of the bare and decorated hollow fiber membranes was evaluated by the permeation test module with the configuration schematically shown in Fig.3.

The LSF hollow fiber in length of 30 cm was connected successively to the glass tube and silicone tube using high-temperature silicone sealant (Tonsan New Materials and Technology Co., Beijing). A larger quartz tube (18 mm in diameter and 400 mm in length) was used to accommodate the hollow fiber membrane, connected on both sides with small-diameter quartz tubes and sealed with epoxy glue. The permeation test module was put in a tubular furnace with inside diameter of 22 mm and effective heating length of 50 mm. To avoid the sealing failure of the two joints with organic sealant were kept 50 mm away from the high temperature zone of the furnace. Air was fed into the

shell side of the test module and helium was passing through the hollow fiber lumen side to collect the permeated oxygen.[33] The gas flow rates were measured by mass flow controllers (D08-8B/ZM, Shanxi Chuangwei, China) and calibrated by a soap bubble flow meter. The composition of the permeated gas was monitored online using a gas chromatograph (Agilent 6890N) fitted with a 5 Å molecular sieve column (3 mm in diameter and 3 m in length) and a TCD detector. Highly pure argon with the flow rate of 40 ml·min^{-1} was used as the carrier gas. Oxygen permeation tests were carried out by varying the helium gas flow rate between 100-300 ml·min^{-1} under the operating temperature between 700-1000 °C.

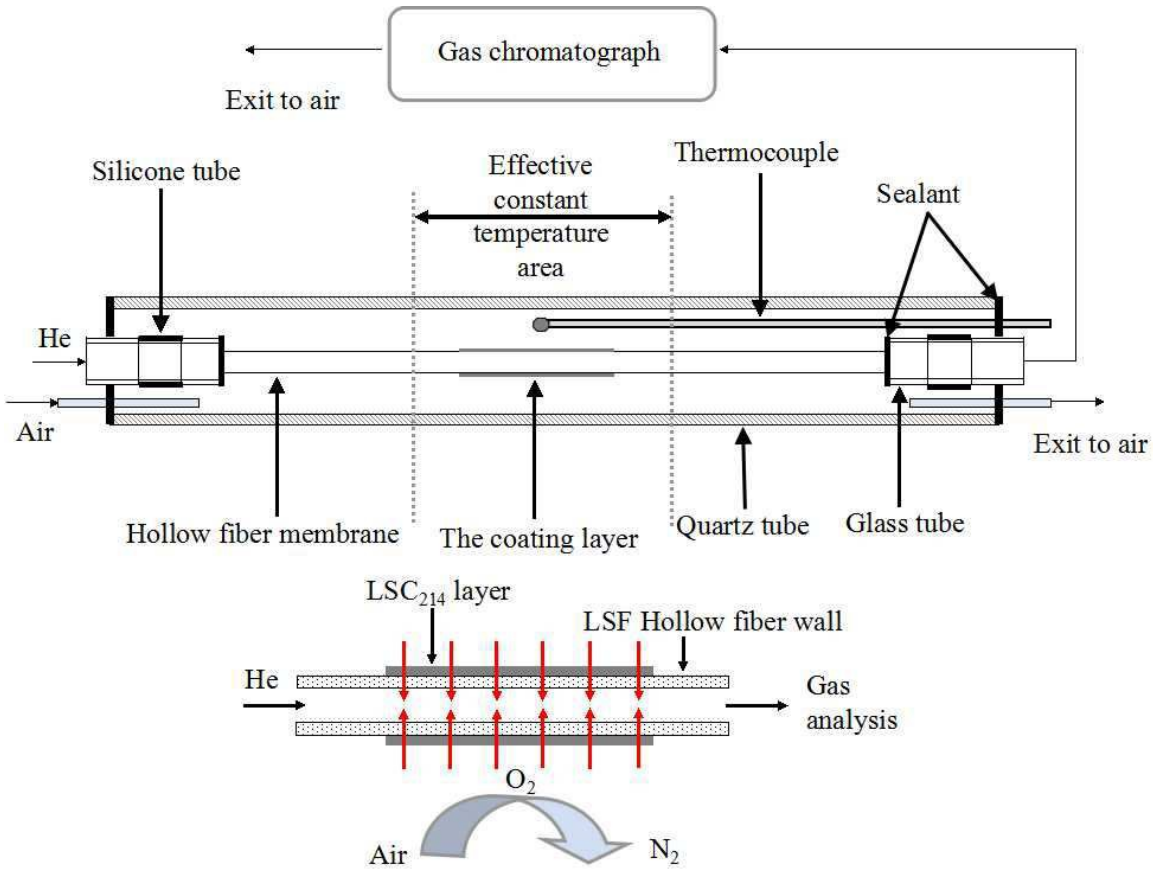

Fig.3. Schematic diagram of oxygen permeation test module and magnified image of LSC_{214} decorated area

The oxygen permeation flux is calculated by

$$J_{O_2} = \frac{V(x_{O_2} - (21/78)x_{N_2})}{A_m}$$

Where  is the permeate gas flow rate (ml·min^{-1}),  and  are the oxygen and nitrogen concentrations in the permeate stream (%). A_m (cm^2), the effective membrane area, is calculated by $A_m = \frac{\pi(D_o - D_i)L}{\ln(D_o / D_i)}$, in which L, D_o and D_i are the effective length for oxygen permeation, outer diameter and inner diameter of the hollow fiber membrane, respectively.[34] All the values of oxygen permeation fluxes and other gas flow rates were calculated on the basis of standard temperature and pressure (STP), and at least three measurements were conducted for each experimental condition. The leakage percentage of the oxygen through the area sealed at high temperatures was less than 0.5% for all experiments.

To further investigate the influence of surface decoration on oxygen permeation performance of LSF membrane, the improvement factor of oxygen flux for the acid-etched and LSC_{214}-decorated LSF hollow fiber membranes were calculated according to the formula as follows:

$$\text{Enhancement Factor} = \frac{J^*_{O_2} - J_{O_2}}{J_{O_2}}$$

Where $J^*_{O_2}$ is the oxygen permeation flux through the modified LSF membrane by acid-etching or LSC_{214} decoration and J_{O_2} is the oxygen permeation flux through the unmodified LSF membrane at the same operating conditions of temperature and sweep gas flow rate.

2.5 Characterization techniques

The crystal phases of the LSF hollow fiber membrane and LSC_{214} powder were determined by X-ray diffraction method (XRD, BRUKER D8 ADVANCE) using a Cu-Kα monochromatized radiation source, which reveal that LSF and LSC_{214} had retained the standard structure. Continuous scan mode was used to collect 2θdata from 20° to 80°with each step 0.02° and 0.1 s. The X-ray tube voltage and current were set at 40 kV and 30 mA, respectively. All the XRD testes were taken under similar condition. The morphology and microstructures of the original and modified hollow fiber membranes were studied using scanning electron microscope (SEM, FEI SIRION 200). Gold sputter coating was performed on the samples under vacuum before the SEM characterization.

3. Results and discussion

3.1 Materials characterization

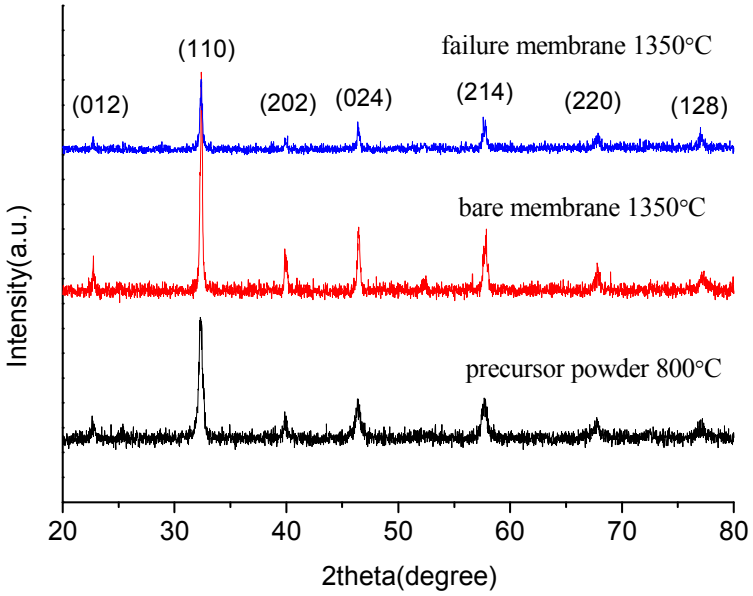

Fig.4. XRD patterns of the LSF powder and hollow fiber membranes

X-ray diffraction (XRD) patterns of the sintered LSF powder, original pure LSF membrane and the failure LSF membrane are shown in Fig.4. The characteristic peaks of the LSF powder calcined at 800 ℃ agree very well with the standard XRD patterns of rhombohedral perovskite phase (JCPDS: 82-1962, 49-0285),[35,36] no other characteristic peaks can be detected in the XRD pattern of the blank LSF membrane and the exhausted membrane at 1350 °C. In addition, the intensity of the corresponding characteristic peaks of the hollow fiber membranes is much larger than the powder, implying that the crystallinity of the LSF sintered at 1350℃ is much better than the powder calcined at 800 ℃.

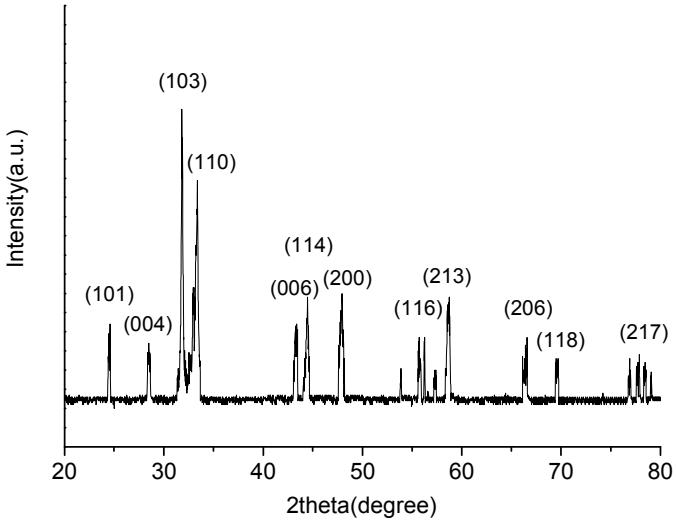

Fig.5. XRD pattern of the LSC_{214} powder (T=1000 °C)

It is well known that in K_2NiF_4-type A_2BO_4 composite oxides, the radii of A and B ions should fulfill the following requirement:[37]

R_A/R_B=1.7-2.4

As the structure factors of La_2CoO_4 and $(La_{0.5}Sr_{0.5})_2CoO_4$ satisfy this relationship, both of them can form the K_2NiF_4-type structure under appropriate conditions.

In general, the K_2NiF_4-type composite oxide crystallizes into two phases,[38,39] i.e. orthorhombic phase (space group: Fmmm) and tetragonal phase (space group: I4/mmm). Fig.5 shows XRD pattern of the LSC_{214} powder sintered at 1000 °C, which appears to be of the orthorhombic phase (JCPDS:72-0937). The partial substitution of La^{3+} by Sr^{2+} in the La_2CoO_4 lattice has been realized successfully.

3.2 Morphology of the hollow fiber membranes

The SEM micrographs of the bare and surface-decorated LSF hollow fiber membranes are shown in Fig.6, which shows that LSF-a and LSF-b exhibit different microstructures. The microstructure formation of hollow fiber membrane is determined by the solvent-nonsolvent exchange rates during phase separation when the polymer solution meets the coagulant. When deionized water is used as the internal coagulant, the solvent-nonsolvent exchange rate on the inner surface is close to that on the outer surface, resulting in the similar microstructure in the inner and outer regions of the cross section (Fig.6(a)). Short finger-like pores are present near the outer and inner walls of the fiber, and a dense layer with a thickness of 40μm is present at the center region. This sandwich structure is attributed to the rapid precipitation at inner and outer layer and slow precipitation at sublayer. However, when NMP-EtOH is used as internal coagulant, the solvent-nonsolvent exchange rate on the inner side may be retarded, leading to the formation of more numerous and longer finger-like pores (Fig.6(b),(c)), which almost across the whole wall of hollow fiber membrane, a thin dense layer with thickness less than 8μm remains (Fig.6(d)). Many short microchannels can be observed near the outer surface because of the possible back flow of the solvent, but these bring little influence on external surface (Fig.6(e),(f)). LSF grain boundaries can be clearly seen. Although some cavities emerge, all of them are isolated pores and no thorough porosities can be detected by the nitrogen leakage test under the pressure difference of 2 bar at room temperature. Fig.6(h) indicates that some pores with diameter of 20~50 μm are formed on the inner

surface of LSF-b, extending to the fiber body, which are expected to increase the oxygen permeation flux greatly. Compared with the deionized water (Fig.6(g)), the distinct effect of NMP-EtOH as internal coagulant on the morphology of inner surface can be clearly recognized.

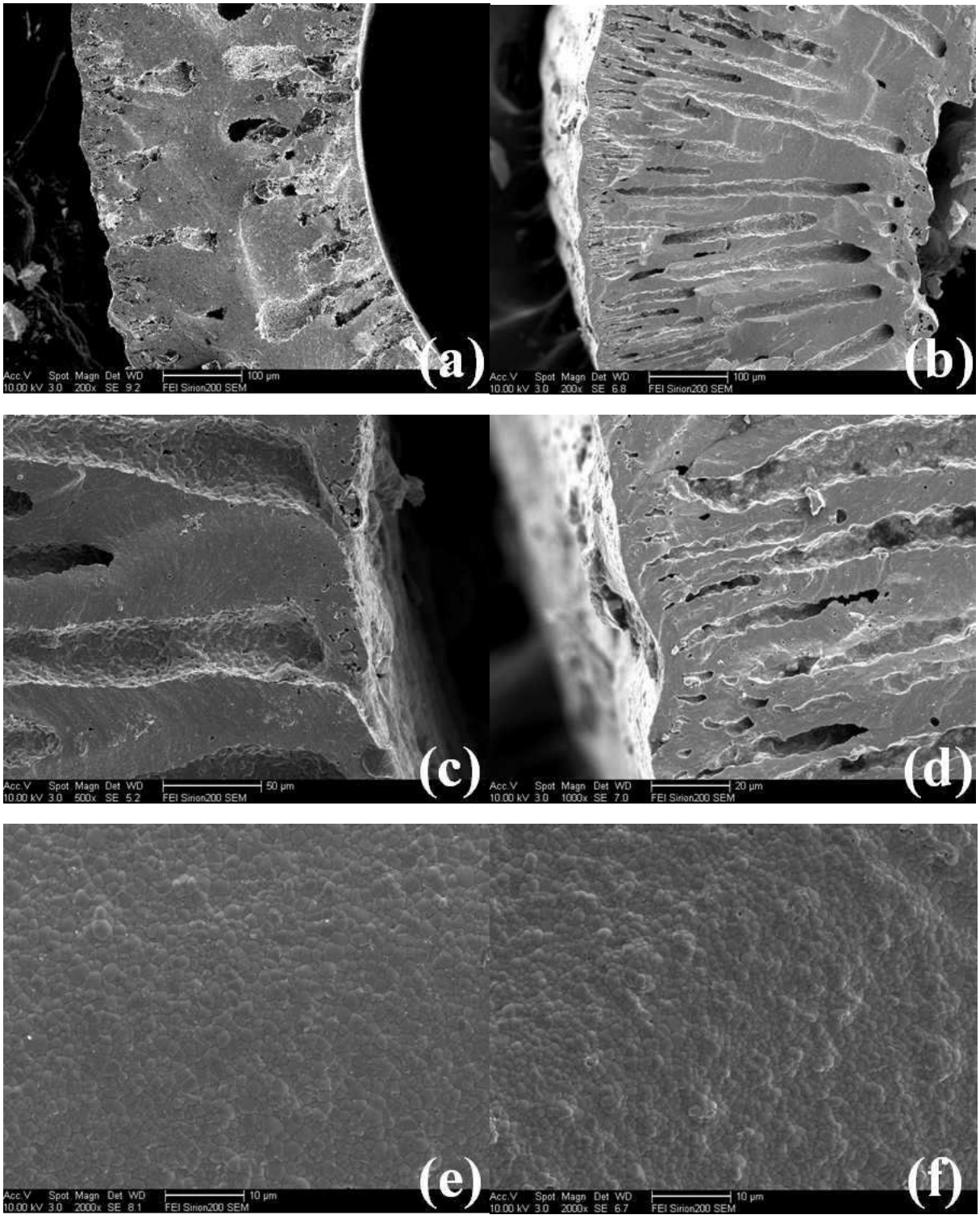

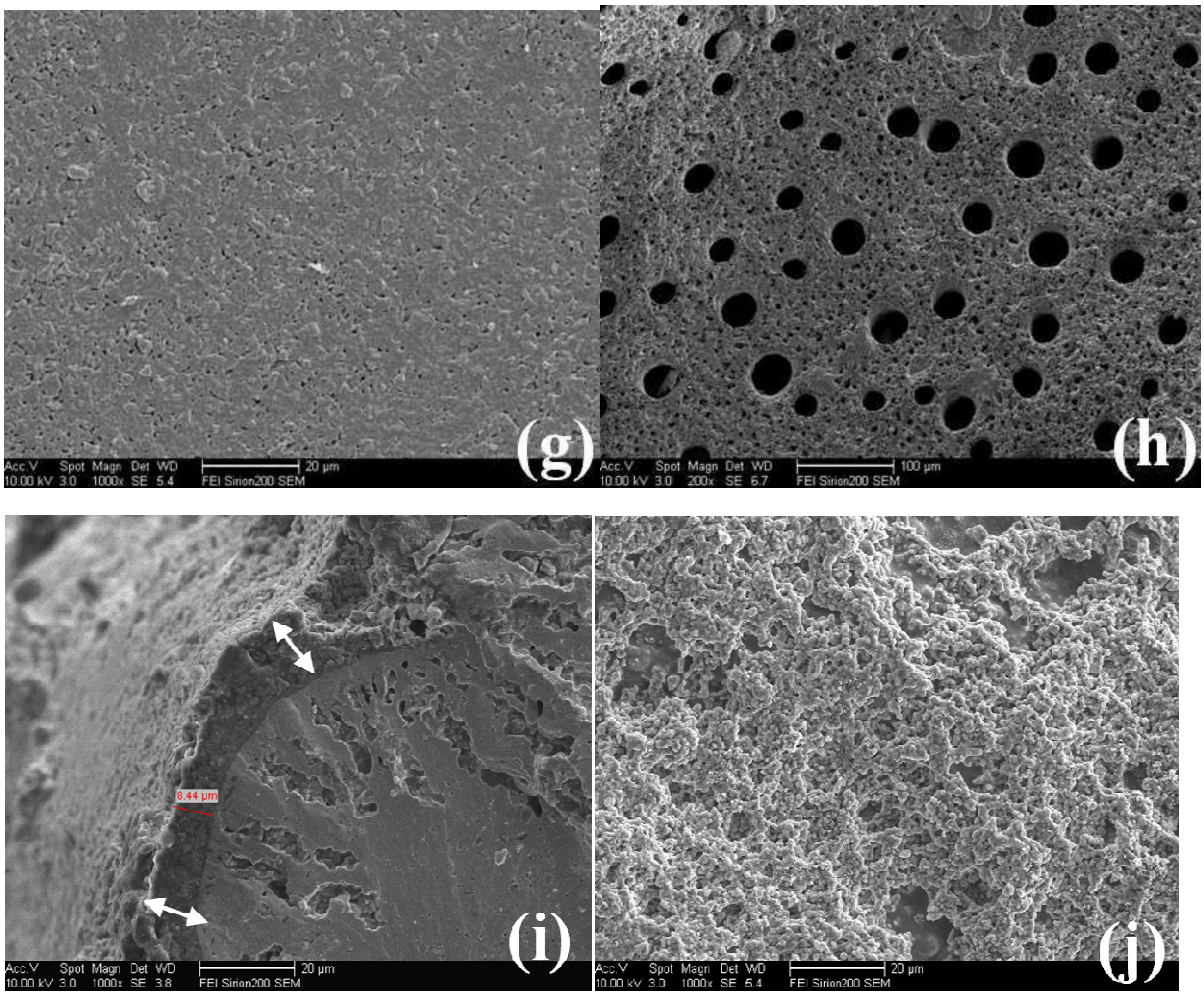

Fig.6. SEM micrographs of LSF hollow fiber membranes with different microstructures. (a) & (b) cross sections of LSF-a and LSF-b, (c) & (d) partial magnification of LSF-b, (e) & (f) external surfaces of LSF-a and LSF-b, (g) & (h) inner surfaces of LSF-a and LSF-b, (i) & (j) cross section & external surface of modified LSF hollow fiber membranes.

Furthermore, we also investigated the effects of the outer surface decoration on the oxygen permeability of perovskite hollow fiber membranes. The K_2NiF_4-type composite oxide LSC_{214} was used for decoration of the gas-tight LSF hollow fiber membranes by single dip-coating method. To demonstrate the changes of surface morphology, the SEM micrographs of modified LSF hollow fiber membrane are shown in Fig.6(i),(j). The LSC_{214} phase with thickness of about 8 μm (marked by arrow in Fig.6(i)) was deposited on the outer surface of the membrane in a discontinuous manner as some areas of bare membrane domains with clear LSF grains could be detected (Fig.6(j)). The LSC_{214} particles fused and dispersed uniformly on the outer surface of membrane were perfectly

integrated with the LSF membrane substrate. Such a well-integrated interface condition is favorable for the formation and extension of triple-phase boundary (TPB), bringing the LSF phase, LSC_{214} phase and air phase converged together. Recent research indicates this can greatly minimize the boundary resistance of oxygen ions immigration and enhance the surface exchange kinetics of oxygen.[23,24] Thus we hypothesize that the LSC_{214}-decorating layer may improve the oxygen permeation rate greatly owing to its high catalytic activity for surface reactions.

3.3 Oxygen permeation performance of the hollow fiber membranes

Before the oxygen permeation measurement, the gas-tightness property of the hollow fiber membranes was evaluated by nitrogen leakage experiment. Both LSF-a and LSF-b are gas-tight hollow fiber membranes (the gas leakage data are 8.8×10^{-8} and 9.7×10^{-7} $mol \cdot m^{-2} \cdot Pa^{-1} s^{-1} \cdot$, respectively) at the same sintering temperature of 1350 °C.

Experimental results of oxygen permeation fluxes varying with the flow rates of sweep gas at different operating temperatures are shown in Fig.7 and Fig.8. It can be seen that the oxygen permeation performance of the LSF-b membrane is much better than that of LSF-a membrane at all the tested conditions, and the LSC_{214}-decoration on the outer surface further increases the oxygen permeation flux greatly. In addition, the operating temperature has a greater effect on the oxygen permeation performance of all these tested LSF membranes than the flow rate of sweep gas.

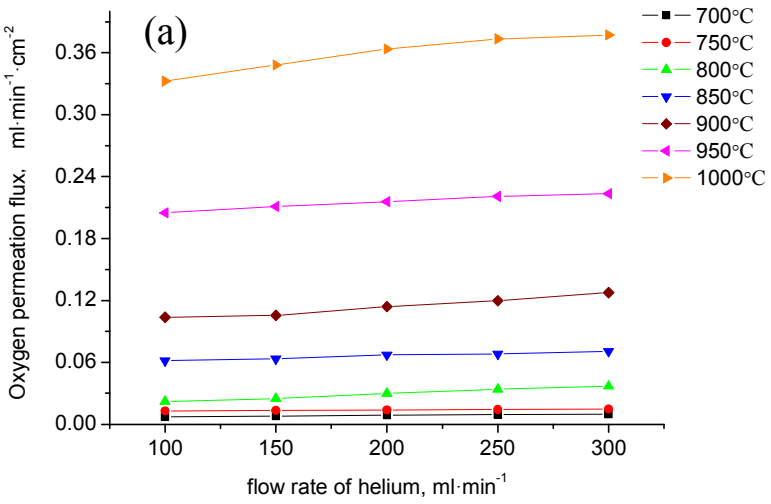

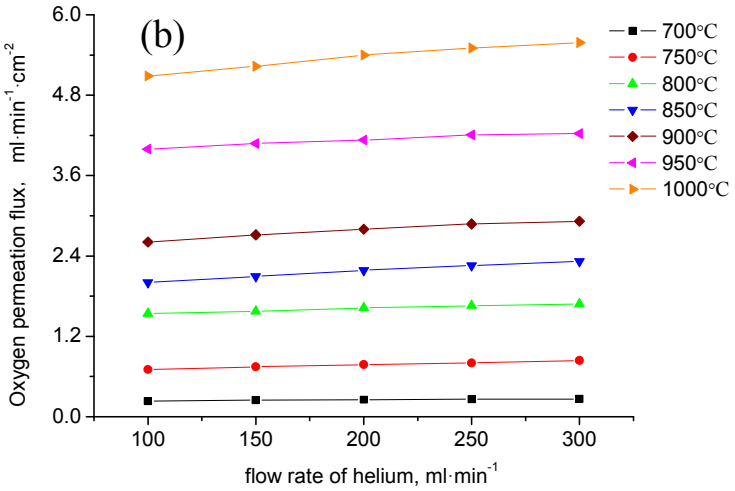

Fig.7. The variation of oxygen permeation fluxes of bare LSF hollow fiber membranes along with the increasing sweep rate of helium gas and temperature. (a) LSF-a membrane, (b) LSF-b membrane. Condition: air feed flow rate = 200 ml·min^{-1}

Fig.7 shows that, with the flow rate of helium gas at a constant of 150 ml·min^{-1}, for example, the oxygen fluxes though the LSF-a and LSF-b membranes had been improved dramatically from 0.008 to 0.348 and 0.246 to 5.233 ml·min^{-1}·cm^{-2}, respectively, when the operating temperature was raised from 700 to 1000 °C. Keeping operating temperature at 1000 °C, for instance, the oxygen permeation fluxes though the LSF-a and LSF-b membranes had been enhanced gradually from 0.322 to 0.377 and 5.088 to 5.586 ml·min^{-1}·cm^{-2}, respectively, when the flow rate of helium gas was adjusted from 100 to 300 ml·min^{-1}·cm^{-2}. LSF-b hollow fiber membrane with one dense layer near the outer surface integrated with the highly porous structure possesses excellent oxygen permeation fluxes, which are about 16 times of those of LSF-a membrane. LSF-b with new microstructure improved the bulk diffusion of oxygen ion greatly, resulting in the increased oxygen permeation flux. This suggests that the microstructure of the hollow fiber membrane plays a crucial role in the oxygen permeation through the perovskite membrane. It can be explained below. When deionized water is used as the bore fluid, three dense layers and two porous layers are formed in the cross section, where the micropores are enclosed by the dense layers. Therefore, the oxygen permeation has to undergo six steps of surface oxygen exchange reaction with short diffusion path. While NMP-EtOH

is added into the bore fluid, the dense layers of lumen side and central part tend to disappear, thus four steps of surface oxygen exchange reaction are eliminated finally.

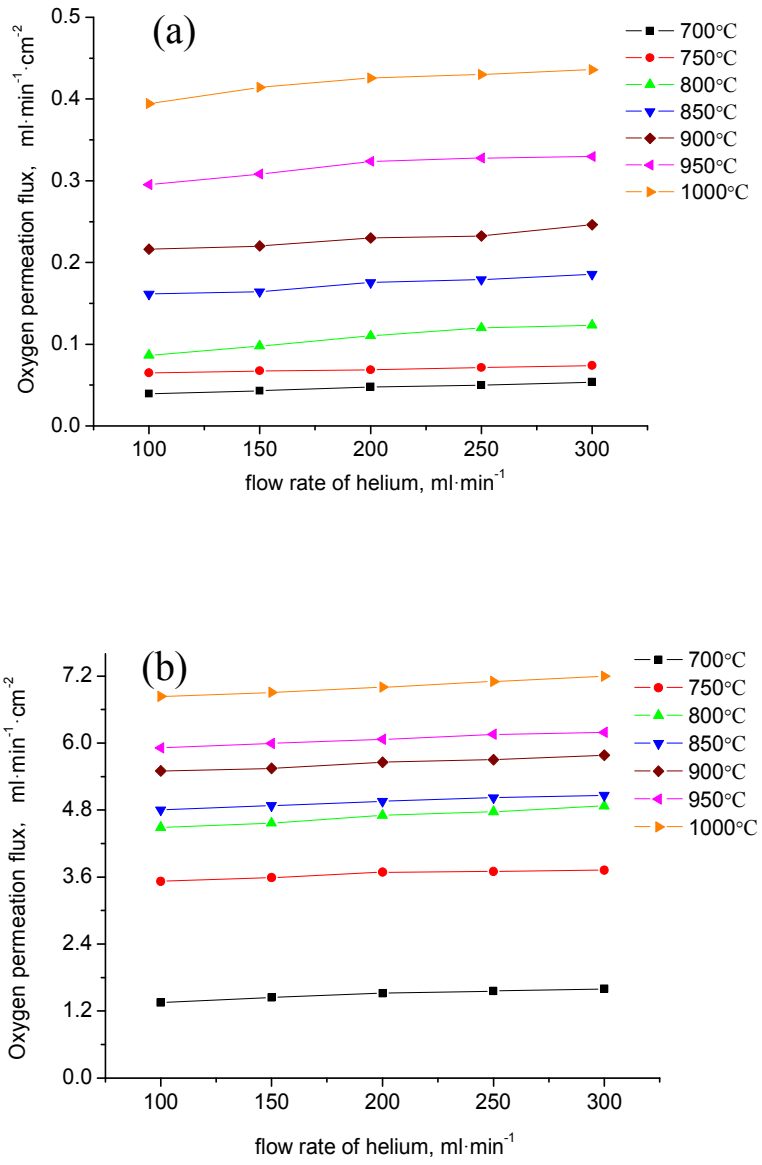

Fig.8. The variation of oxygen permeation fluxes of the LSC_{214}-coated LSF hollow fiber membranes along with the increasing sweep rate of helium gas and temperature. (a) LSC_{214}-decorated LSF-a hollow fiber membrane，(b) LSC_{214}-decorated LSF-b hollow fiber membrane.

After the LSC_{214} modification, it can be seen from Fig.8 that the maximal oxygen permeation

flux of LSF-b hollow fiber membrane is about 7.199 $ml \cdot min^{-1} \cdot cm^{-2}$, which is almost 1.3 times of the bare LSF-b membrane (5.586 $ml \cdot min^{-1} \cdot cm^{-2}$) and 19 times of the bare LSF-a membrane (0.377 $ml \cdot min^{-1} \cdot cm^{-2}$) at the same conditions (flow rate of helium: 300 $ml \cdot min^{-1}$; temperature: 1000 °C). After the outer surface modification, the porous LSC_{214} coating layer not only provides higher specific surface area to facilitate diffusion and adsorption of oxygen molecules on the surface, but also enhances the surface exchange reaction rate of oxygen ion remarkably (i.e. higher catalytic activity).

The operating temperature has a great influence on the oxygen permeation performance. For example (Fig.7 and 8), keeping the flow rate of helium gas at 200 $ml \cdot min^{-1}$, the oxygen permeation fluxes though the bare and the LSC_{214}-decorated LSF-a membranes enhanced from 0.009 to 0.367 and 0.048 to 0.426 $ml \cdot min^{-1} \cdot cm^{-2}$, respectively, with operating temperature varied from 700 to 1000 °C. Meanwhile, the oxygen permeation fluxes of the bare and the LSC_{214}-decorated LSF-b membranes climbed from 0.254 to 5.401 and 1.520 to 7.003 $ml \cdot min^{-1} \cdot cm^{-2}$, respectively.

In addition, it also can be seen that the oxygen permeation fluxes are positively associated with the flow rates of helium gas. For instance (Fig.7 and 8), keeping operating temperature at 1000 °C, the oxygen permeation fluxes through the bare and the LSC_{214}-decorated LSF-a membranes raised from 0.32 to 0.38 and 0.39 to 0.44 $ml \cdot min^{-1} \cdot cm^{-2}$, respectively, with the flow rate of helium gas changed from 100 to 300 $ml \cdot min^{-1}$. At the same time, the oxygen permeation fluxes of the bare and the LSC_{214}-decorated LSF-b membranes improved from 5.09 to 5.59 and 6.84 to 7.20 $ml \cdot min^{-1} \cdot cm^{-2}$, respectively.

For the commercial consideration, 1 $ml \cdot min^{-1} \cdot cm^{-2}$ is regarded as the threshold value of oxygen permeation flux,[40] which LSF-b bare membrane could reach even no more than 800 °C. By coating a porous LSC_{214} layer on the outer surface of LSF-b membrane, this target can be achievable operated below 700 °C.

By comparison of the effects of the sweep gas flow rate and operating temperature, we can comment that the operating temperature parameter plays a crucial role on the oxygen permeability property of all these LSF membranes. Thus the driving forces for oxygen permeation through the mixed conducting ceramic membranes are associated not only with the oxygen partial pressure gradient but also with the temperature. To some extent, oxygen permeation is a temperature determining process.

Furthermore, the effect of surface decoration on oxygen permeation performance was also explored by the enhancement factor, which were calculated and plotted against operating temperature and sweep gas rates in Fig.9. As temperature increases from 700 °C to 1000 °C, both LSF-a and LSF-b membranes present the same trend on the enhancement factor variation of the oxygen permeation flux. At intermediate temperatures 700 °C, 750 °C, 800 °C, the oxygen flux enhancement factors of LSF-a (LSF-b) membrane are about 4.5, 4.0, 3.0 (5.0, 4.0, 1.9), respectively, while temperature reaches 1000 °C, that of the LSF-a (LSF-b) membrane reduces enormously to 0.15 (0.29). These results show that the permeation enhancement factor always decreases with increasing temperature and are less related to the sweep gas rates on the whole. For both kinds of decorated membranes, it can be easily identified that more remarkable improvements of oxygen permeation fluxes appear at intermediate operating temperature range (700-850 °C) than higher temperature range (850-1000 °C).[41,42]

The oxygen permeation rate is usually determined by bulk diffusion process and the surface exchange reaction of oxygen. The phenomenon described above implies that the rate-determining step of the oxygen permeation process varies with the change of operating temperature. At lower temperatures, the oxygen permeation is mainly controlled by the rate of surface exchange reaction. However, along with the increase of temperature, the rate-determining role of the bulk oxygen diffusion gradually predominates over that of the surface exchange reaction because the activation energy of bulk diffusion is much larger than that of surface exchange reaction. As a result, the enhancement factor of oxygen permeation flux by surface decoration is relatively reduced.

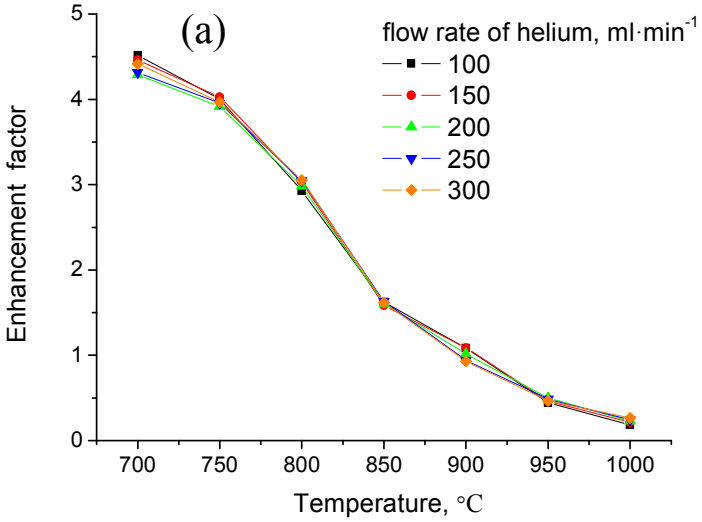

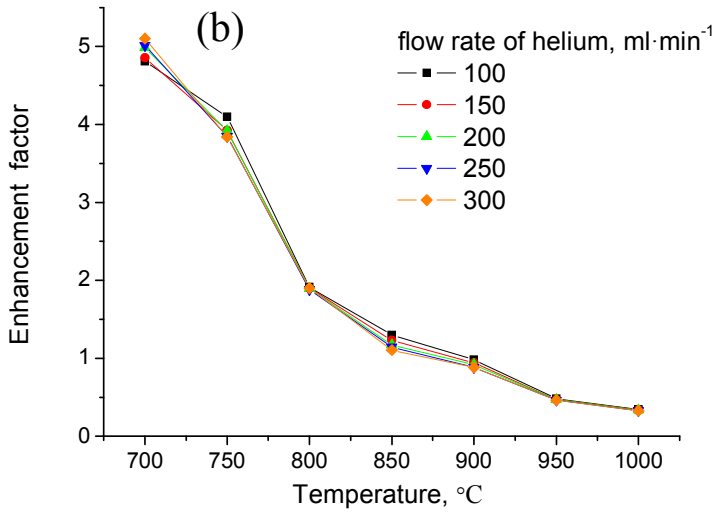

Fig.9. The enhancement factors of oxygen permeation fluxes for LSC_{214}-decorated LSF hollow fiber membranes against operating temperature at different sweep gas rates. (a) LSC_{214}-decorated LSF-a hollow fiber membrane, (b) LSC_{214}-decorated LSF-b hollow fiber membrane. Condition: air feed flow rate= 200 ml·min^{-1}.

3.4 Apparent activation energy of oxygen permeation process

To further investigate the surface decoration effect of LSC_{214} layer on the oxygen permeability of LSF hollow fiber membranes from kinetic points of view, Arrhenius plots and apparent activation energy were employed here.[43-45]

Fig.10 demonstrates Arrhenius plots of the oxygen permeation flux through all kinds of LSF hollow fiber membranes as a function of operating temperature at a constant helium flow rate of 100 ml·min^{-1}. For both kinds of membranes with different microstructures, LSF-a and LSF-b, apparent activation energies of oxygen permeation through the LSC_{214}-decorated membranes are much lower than those through the bare ones. Overall, the apparent activation energy of LSC_{214}-decorated LSF-a (82.67 kJ·mol^{-1}) is less than that of the bare LSF-a (138.55 kJ·mol^{-1}), similarly, that of the coated LSF-b (44.54 kJ·mol^{-1}) is also smaller than the bare LSF-b (95.88 kJ·mol^{-1}). Comparing bare LSF-a with bare LSF-b, it can be seen that the LSF-b membrane has rather lower apparent activation energy than that of LSF-a, resulting from the quite different microstructures. For both kinds of bare and LSC_{214}-decorated LSF membranes studied here, it is obvious that the apparent activation energies of the modified ones are much lower than those of the bare ones. The surface decoration decreases the

apparent activation energy observably, which agrees well with the previous study.

Surface modification provides more surface area (i.e. active sites) than the original LSF membrane to improve the surface oxygen reduction reaction kinetics, resulting in the decrease of apparent activation energies. Besides the high specific surface area effect, the high catalytic activity of LSC_{214}-decoration significantly raises the surface exchange reaction rate of oxygen, therefore the apparent activation energies further reduced dramatically. This study thus offers a new strategy to improve the oxygen permeability of hollow fiber membranes by K_2NiF_4-type composite oxide surface decoration. As described above, the mechanism of oxygen permeation through the hollow fiber membrane is very complicated. The hollow fiber membranes with long finger-like pores show a great potential on oxygen permeation. Detailed explanation and understanding of the mechanism behind this complex process is desperately needed now. Only in this way, new oxygen transport materials with better performance could be designed and prepared for applications, such as oxygen permeation membrane, SOFC cathode, oxygen sensor, and so on. For that reason, we will investigate the oxygen transport mechanism in detail next by using first principle calculation method at the atomic level.

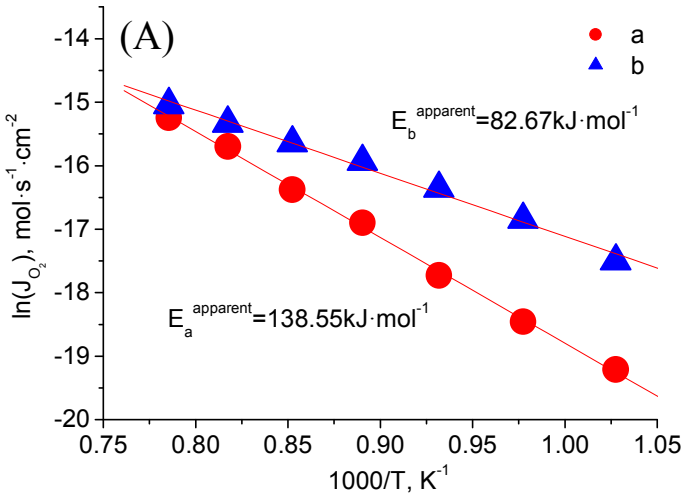

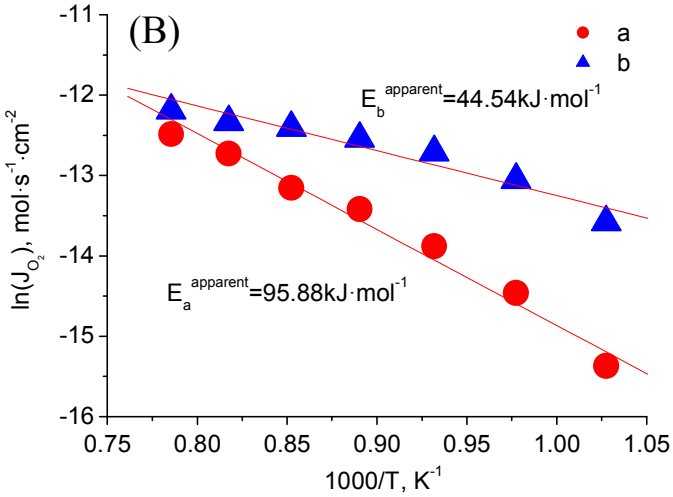

Fig.10. Arrhenius plots of the oxygen permeation flux through the LSF hollow fiber membranes. (A) LSF-a; (B) LSF-b; a: bare membrane; b: LSC_{214}-decorated membrane. Conditions: temperature varies from 700 °C to 1000 °C; air flow rate= 200 ml·min^{-1}; Helium flow rate= 100 ml·min^{-1}.

3.5 Stability test

To be a good membrane material for oxygen permeation, it should have not only sufficient high oxygen permeation flux, but also good stability for long term operation under certain oxygen partial pressure. Long-term operation tests on the bare and LSC_{214}-decorated LSF-b hollow fiber membranes were conducted under the condition as follows: T= 900 °C, flow rate of sweep gas = 100 ml·min^{-1} and air flow rate = 200 ml·min^{-1}. The oxygen permeation fluxes plotted against operating time were shown in Fig.11. It can be observed that the oxygen permeation fluxes of LSF-b membrane systems keep steady, varying from 2.516 to 2.619 ml·min^{-1}·cm^{-2} of bare LSF-b and 5.513 to 5.634 ml·min^{-1}·cm^{-2} of modified LSF-b, during the entire operation time more than 300 hours at 900 °C. This implies that the new kind of LSF-b hollow fiber membrane shows high stability at least under these operating conditions.

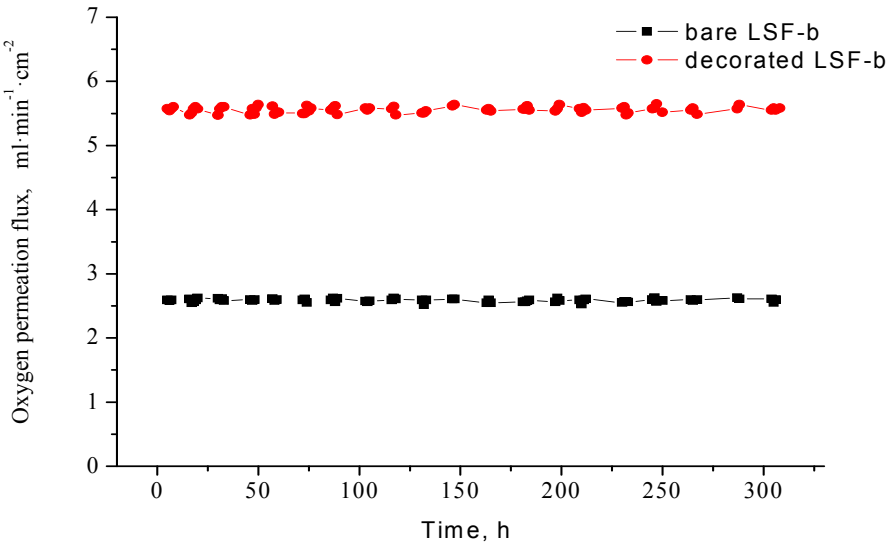

Fig.11. Oxygen permeation fluxes as function of operating time at 900 °C. Conditions: air feed flow rate = 200 ml·min^{-1}, sweep gas flow rate = 100 ml·min^{-1}.

4. Conclusions

In this work, the powders of perovskite oxide LSF and K_2NiF_4-type oxide LSC_{214} were successfully prepared by the sol-gel method, and the gas-tight LSF hollow fiber membranes with two kinds of microstructures (LSF-a and LSF-b) were fabricated via the phase inversion/sintering method. Outer surface decoration with dispersed porous K_2NiF_4-type oxide LSC_{214} was carried out to improve the surface exchange reaction kinetics of oxygen reduction. The main conclusions are as follows:

(1) The undecorated LSF-a and LSF-b membranes have oxygen permeation fluxes of 0.008-0.348 and 0.246-5.233 ml·min^{-1}·cm^{-2}, respectively, in the temperature range of 700 to 1000 °C and the flow rate of helium gas at 150 ml·min^{-1}.

(2) Compared to the undecorated membranes, the oxygen permeation fluxes of the LSC_{214}-decorated LSF-a and LSF-b membranes were improved by 1.2-5.5 and 1.3-6.0 times, respectively, depending on the operating temperatures. More remarkable improvements of oxygen permeation fluxes appear at intermediate operating temperature range (700-850 °C) than higher temperature range (850-1000 °C).

(3) The apparent activation energy of LSC_{214}-decorated LSF-a (82.67 kJ·mol^{-1}) is less than that of

the bare LSF-a (138.55 kJ·mol^{-1}), similarly, that of the coated LSF-b (44.54 kJ·mol^{-1}) is also smaller than the bare LSF-b (95.88 kJ·mol^{-1}).

(4) LSF membranes exhibited high oxygen permeation stability during the entire investigated 300 hours at 900 °C without decay, about 2.6 ml·min^{-1}·cm^{-2} and 5.6 ml·min^{-1}·cm^{-2} for the undecorated and LSC_{214}-decorated LSF-b membranes, respectively.

Acknowledgements

The authors gratefully acknowledge the financial supports for this work provided by Shandong Provincial Natural Science Foundation (No. ZR2012BQ010)，the Scientific Research Foundation for the Returned Overseas Chinese Scholars (State Education Ministry of China) and the National Natural Science Foundation of China (21176146).

References

1 X. Zhu, H. Liu, Y. Cong, W. Yang, *Chem. Commun*., 2012, **48**, 251-253.

2 N.H. Othman, Z. Wu, K. Li, *J. Membr. Sci.,* 2014, **468**, 31-41.

3 Runze Wang , Bo Meng, Xiuxia Meng , Xiaoyao Tan , Jaka Sunarso , Lihong Liu , Shaomin Liu, *J. Membr. Sci.,* 2015, **479**, 232-239.

4 Z. Wang, Y. Kathiraser, T. Soh, S. Kawi, *J. Membr. Sci.,* 2014, **465**, 151-158.

5 Y. Liu, X. Zhu, M. Li, H. Liu, Y. Cong, W. Yang, *Angew. Chem., Int. Ed.,* 2013, **52**, 3232-3236.

6 E. J. Crumlin, E. Mutoro, W. T. Hong, M. D. Biegalski, H. M. Christen, Z. Liu, H. Bluhm, Y. Shao-Horn, *J. Phys. Chem. C.,* 2013,**117**, 16087-16094.

7 G. M. Rupp, A. Limbeck, M. Kubicek, A. Penn, M. S. Pollach, G. Friedbacher, J. Fleig, *J. Mater. Chem. A,* 2014, **2**, 7099 −7180.

8 S. B. Adler, X. Y. Chen, J. R. Wilson., *J. Catal.*, 2007, **245**, 91 −109.

9 Y. L. Lee, J. Kleis, J. Rossmeisl, D. Morgan, *Phys. Rev. B.,* 2009, **80**, 224101,1 −20.

10 A. Tarancon, M. Burriel, J. Santiso, S. J. Skinner, J. A. Kilner, *J. Mater. Chem.,* 2010, **20**, 3799 −3813.

11 H. Luo, T. Klande, Z. Cao, F. Liang, H. Wang, *J. Caro, J. Mater. Chem. A.,* 2014, **2**, 7780-7787.

12 H. Taguchi, H. Kido, M. Kato, K. Hirota, *Mater. Res. Bull.,* 2015, **64**, 318 −322.

13 C.T. Haihui Wang, Armin Feldhoff and JÜrgen Caro, *Adv. Mater.*, 2005, **17**, 1785-1788.

14 X. Dong, Z. Xu, X. Chang, C. Zhang, W. Jin, *J. Am. Ceram. Soc.*, 2007, **90**, 3923-3929.

15 D. Schlehuber, E. Wessel, L. Singheiser, T. Markus, *J. Membr. Sci.,* 2010, **351**, 16-20.

16 J. Sunarso, S. Baumann, J.M. Serra, W.A. Meulenberg, S. Liu, Y.S. Lin, J.C. Diniz da Costa, *J. Membr. Sci.,* 2008, **320**, 13-41.

17 X. Tan, Z. Wang, H. Liu, S. Liu, *J. Membr. Sci.,* 2008, **324**, 128-135.

18 Y. Wei, Q. Liao, Z. Li, H. Wang, *Sep. Purif. Technol*., 2013, **110**, 74-80.

19 S.S. Adrian Leo , Shaomin Liu ,João C. Diniz da Cost, *J. Membr. Sci.,* 2010, **368**, 64-68.

20 T. Kida, S. Ninomiya, K. Watanabe, N. Yamazoe, K. Shimanoe, *ACS Appl. Mater. Interfaces*., 2010, **2**, 2849-2853.

21 S.L. A. Leo, J.C. Diniz da Costa, Z. Shao, *Sci. Technol. Adv. Mat*., 2006, **7**, 819-825.

22 A. Thursfield, I.S. Metcalfe, *J. Membr. Sci.,* 2007, **288**, 175-187.

23 J.W. Han, B. Yildiz, *Energy Environ. Sci*., 2012, **5**, 8598-8607.

24 E. Mutoro, E.J. Crumlin, M.D. Biegalski, H.M. Christen, Y. Shao-Horn, *Energy Environ. Sci*., 2011, **4**, 3689-3696.

25 L. Wang, S. Imashuku, A. Grimaud, D. Lee, K. Mezghani, M.A. Habib, Y. Shao-Horn, *Ecs Electrochem Lett*., 2013, **2**, 77-81.

26 H. Dulli, P. A. Dowben, S. H. Liou, E. W. Plummer, *Phys. Rev. B: Condens. Matter.,* 2000, **62**, 14629–14632.

27 K. Szot, W. Speier, *Phys. Rev. B: Condens. Matter.,* 1999, **60**, 5909–5926.

28 E. J. Crumlin, E. Mutoro, S. J. Ahn, G. Joselao, D. N. Leonard, A. Borisevich, M. D. Biegalski, H. M. Christen, Y. Shao-Horn, *J. Phys. Chem. Lett.,* 2010,**1**, 3149-3155.

29 Y.L, X. Tan, K. Li, *Ind. Eng. Chem. Res*., 2005, **44**, 61-66.

30 L. Ge, R. Ran, Z. Shao, Z. H. Zhu, S. Liu, *Ceram. Int.,* 2009, **35**, 2809–2815.

31 Z. Wang, N. Yang, B. Meng, X. Tan, K. Li, *Ind. Eng. Chem. Res.,* 2009, **48**, 510-516.

32 X. Tan, Y. Liu, K. Li, *AIChE J.*, 2005, **51**, 1991-2000.

33 J. Hong, P. Kirchen, A.F. Ghoniem, *J. Membr. Sci.,* 2013, **428**, 309-322.

34 X.Tan, Z.W and .K. Li, *Ind. Eng. Chem. Res*., 2010, **49**, 2895-2901.

35 D.B.C. S.E.Dann, M.T.Weller, M.F.Thomas, A.D.Al-Rawwas, *J. Solid. State. Chem.*, 1994, **109**,134-144.

36 J.B. Johan E. ten Elshof, *Powder Diffraction J*., 1996, **11**,240-245.

37 D. Ganguli, *J. Solid. State. Chem.*, 1979, **30**, 353-356.

38 H.M.-B. U. Lehmann, *Zeitschrift für anorganische und allgemeine Chemie.*, 1980, **470**, 59-63.

39 I.I.V. M. V. Kniga, E. E. Klementoviah, *Russ. J. Inorg. Chem.*, 1979, **24.**

40 B.C.H. Steele, *Mat. Sci. Eng. B-Solid*., 1992, **13**, 79-87.

41 D. Han, J. Wu, Z. Yan, K. Zhang, J. Liu, S. Liu, *RSC Adv.*, 2014, **4**, 19999-20004.

42 Z. Wang, H. Liu, X. Tan, Y. Jin, S. Liu, *J. Membr. Sci.,* 2009, **345**, 65-73.

43 J.M. Serra, J. Garcia-Fayos, S. Baumann, F. Schulze-Küppers, W.A. Meulenberg, *J. Membr. Sci.,* 2013, **447**, 297-305.

44 H. Huang, S. Cheng, J. Gao, C. Chen, J. Yi, *Mater. Lett*., 2014 **137**, 245-248.

45 T.T. Norton, J. Ortiz-Landeros, Y.S. Lin, *Ind. Eng. Chem. Res*., 2014, **53**, 2432-2440.